Oncogene (2005) 24, 4037–4051

www.nature.com/onc

A functional heparan sulfate mimetic implicates both heparanase and heparan sulfate in tumor angiogenesis and invasion in a mouse model of multistage cancer

Johanna A Joyce*[,1], Craig Freeman[2], Nicole Meyer-Morse[1], Christopher R Parish[2] and Douglas Hanahan*[,1]

[1]*Department of Biochemistry and Biophysics, Diabetes and Comprehensive Cancer Centers, University of California at San Francisco, 513 Parnassus Avenue, San Francisco, CA 94143-0534, USA;* [2]*Division of Immunology and Genetics, The John Curtin School of Medical Research, The Australian National University, PO Box 334, Canberra, ACT, 2601 Australia*

Heparan sulfate proteoglycans are integral components of the extracellular matrix that surrounds all mammalian cells. In addition to providing structural integrity, they act as a storage depot for a variety of heparan sulfate (HS)-binding proteins, including growth factors and chemokines. Heparanase is a matrix-degrading enzyme that cleaves heparan sulfate side chains from the core proteoglycans, thus liberating such HS-binding proteins, as well as potentially contributing to extracellular matrix degradation. Here, we report that heparanase mRNA and protein expression are increased in the neoplastic stages progressively unfolding in a mouse model of multistage pancreatic islet carcinogenesis. Notably, heparanase is delivered to the neoplastic lesions in large part by infiltrating Gr1+/Mac1+ innate immune cells. A sulfated oligosaccharide mimetic of heparan sulfate, PI-88, was used to inhibit simultaneously both heparanase activity and HS effector functions. PI-88 had significant effects at distinct stages of tumorigenesis, producing a reduction in the number of early progenitor lesions and an impairment of tumor growth at later stages. These responses were associated with decreased cell proliferation, increased apoptosis, impaired angiogenesis, and a substantive reduction in the number of invasive carcinomas. In addition, we show that the reduction in tumor angiogenesis is correlated with a reduced association of VEGF-A with its receptor VEGF-R2 on the tumor endothelium, implicating heparanase in the mobilization of matrix-associated VEGF. These data encourage clinical applications of inhibitors such as PI-88 for the many human cancers where heparanase expression is elevated or mobilization of HS-binding regulatory factors is implicated.
Oncogene (2005) **24,** 4037–4051. doi:10.1038/sj.onc.1208602
Published online 4 April 2005

*Correspondence: JA Joyce. Current address: Cancer Biology and Genetics Program, Memorial Sloan Kettering Cancer Center, 1275 York Avenue, Box 372, New York, NY 10021, USA;
E-mail: joycej@mskcc.org or
D Hanahan; E-mail: dh@biochem.ucsf.edu
Received 26 October 2004; revised and accepted 21 January 2005; published online 4 April 2005

Keywords: heparanase; heparan sulfate-binding proteins; invasion; angiogenesis; pancreatic neuroendocrine cancer; mouse model

Introduction

The structural integrity of cells within normal tissues is provided in large part by different classes of macromolecules embedded in underlying basement membranes (BM) and the extracellular matrix (ECM). These include heparan sulfate proteoglycans (HSPGs), collagen, laminin, and fibronectin, which bind to each other, forming an intricate three-dimensional matrix (Hileman *et al*., 1998; Kalluri, 2003; Yurchenco and Schittny, 1990). HSPGs are among the most complex of these structural macromolecules, as they consist of a protein core to which heparan sulfate (HS) side chains are covalently attached. The HS side chains can bind to a variety of proteins, including growth factors, angiogenic proteins, and chemokines, thus providing a local extracellular storage depot in various tissues (Vlodavsky *et al*., 1991; Bernfield *et al*., 1999; Tumova *et al*., 2000). In addition, HSPGs are found on the surface of many cells where they enhance cell signaling, forming ternary complexes between certain growth factors and their cognate receptors (Ornitz, 2000; Powers *et al*., 2000; Schlessinger *et al*., 2000).

During tumor development, these tight structural ECM and BM networks are thought to be remodeled by various matrix-degrading enzymes (e.g. matrix metalloproteases, endoglycosidases, aspartic, cysteine, and serine proteases) to facilitate tumor cell proliferation, angiogenesis, invasion, and metastasis. As part of this process, HSPG turnover may contribute to tumor progression, by releasing sequestered HS-binding proteins, which are now free to signal through their cognate receptors, and by effecting alterations in the BM/ECM that facilitate angiogenesis and tumor invasion. As such, examining the role of the enzymes that mediate HSPG turnover is relevant to understanding the importance of

this process in tumor development. One such enzyme is heparanase, an endoglycosidase that specifically cleaves the HS side chains of HSPGs (Parish *et al*., 2001). Heparanase is expressed in many normal cells, including platelets, neutrophils, activated lymphocytes, astrocytes, and cytotrophoblasts (Freeman and Parish, 1997, 1998; Dempsey *et al*., 2000; Marchetti *et al*., 2000; Haimov-Kochman *et al*., 2002), in addition to malignant carcinoma, melanoma and lymphoma cells (Marchetti and Nicolson, 1997; Marchetti *et al*., 2000; Kim *et al*., 2002; Kelly *et al*., 2003).

Heparanase has been implicated in human cancer, particularly in malignant, aggressive tumors, for a number of years (Parish *et al*., 2001). These data have come largely from correlative studies documenting a positive association between increased heparanase expression or activity and enhanced tumor invasion and metastasis (Hulett *et al*., 1999; Koliopanos *et al*., 2001; Maxhimer *et al*., 2002; Tang *et al*., 2002; Zetser *et al*., 2003). Clinical studies have demonstrated increased heparanase activity in serum from patients with metastatic malignant melanoma (Nakajima *et al*., 1988), and high levels of heparanase expression have been negatively correlated with patient survival (Koliopanos *et al*., 2001; Kim *et al*., 2002; Tang *et al*., 2002). Heparanase upregulation has been reported in a variety of tumors, including pancreatic cancer (Koliopanos *et al*., 2001; Kim *et al*., 2002), gastric carcinoma (Tang *et al*., 2002), lung adenocarcinoma (Uno *et al*., 2001), breast cancer (Vlodavsky *et al*., 1999; Zcharia *et al*., 2001; Maxhimer *et al*., 2002), esophageal carcinoma (Uno *et al*., 2001), and colon cancer (Vlodavsky *et al*., 1999; Friedmann *et al*., 2000).

If growth factor mobilization and alterations of the BM/ECM in such human tumors, following HSPG cleavage by upregulated heparanase, are functionally important, then inhibition of heparanase activity would be expected to antagonize tumor development. We sought to assess the expression and possible functional contributions of heparanase during multistage tumorigenesis in a manipulatable mouse model of cancer. To this end, we chose to use the RIP1-Tag2 mouse model of pancreatic islet β-cell carcinoma, in which the progressive stages of tumorigenesis from normal islets to tumors can be easily identified and manipulated (Hanahan, 1985; Folkman *et al*., 1989). RIP1-Tag2 transgenic mice develop multiple pancreatic islet tumors by 12–14 weeks of age, as a consequence of expressing the SV40T antigen (Tag) oncogenes in insulin-producing β-cells. Tumor development in these mice proceeds through a series of discrete stages, in which approximately 50% of the $\sim$400 islets in the pancreas become hyperproliferative, and a subset of these (40–50 islets, or $\sim$20%) subsequently switch on angiogenesis. In turn, 15–20% of these angiogenic islets develop into solid tumors, either benign, encapsulated lesions or invasive carcinomas. This mouse model has proved useful for examining the effects of various anti-angiogenic and antitumorigenic agents, as it allows these compounds to be tested in a stage-specific manner (Bergers *et al*., 1999). As such, we have been able to discern the role of various matrix-degrading enzymes, endogenous angiogenesis inhibitors, and tyrosine kinase receptors at discrete stages of tumorigenesis (Bergers *et al*., 1999, 2000, 2003; Joyce *et al*., 2004).

In this report, we show that heparanase expression increases during RIP1-Tag2 tumorigenesis, and that the enzyme is predominantly supplied by innate immune cells infiltrating neoplastic tissues. A sulfated oligosaccharide, PI-88 (Parish *et al*., 1999), that inhibits heparanase activity and sequesters mobilized HS-binding regulatory factors was used as a functional probe in therapeutic trials, revealing significant effects on multiple stages of tumorigenesis, reducing the number of early angiogenic progenitor lesions and impairing tumor growth in later stages.

Results

Characterization of heparanase levels during multistep tumorigenesis

To examine the levels of heparanase RNA and protein during multistage tumorigenesis in RIP1-Tag2 mice, we isolated normal islets, angiogenic islets, and tumors, as previously described (Parangi *et al*., 1995). RNA and cDNA were prepared from pools of lesions from these three stages, and real-time quantitative RT–PCR was performed for heparanase and a control housekeeping gene, *mGus* (D'Amore *et al*., 1988). A gradual and significant increase in heparanase RNA expression was observed as normal islets develop into angiogenic islets and subsequently tumors (Figure 1a). Protein lysates were also prepared from the same stages, and Western blot analysis with an anti-heparanase antibody was performed on equally loaded amounts of protein. This method revealed an even more pronounced increase in the amount of heparanase protein in its active form ($\sim$45 kDa) (Figure 1b), suggesting that there may be post-transcriptional or post-translational modifications that affect heparanase protein and/or activity levels in tumors.

As RIP1-Tag2 tumors are composed of multiple cell types, including transformed (Tag+) tumor cells, endothelial cells, and infiltrating innate immune cells (including macrophages and neutrophils), we sought to determine the cellular source of heparanase. The constituent cell types were separated from RIP1-Tag2 tumors by flow cytometry as previously described (Bergers *et al*., 2003). RNA and cDNA were synthesized from approximately 300 000 of each of the three sorted cell types (tumor, endothelial, and Gr-1+/Mac-1+ innate immune cells) and real-time quantitative RT–PCR was performed for heparanase and *mGus*. Relative expression levels of heparanase in each cell type were calculated by normalization to *mGus,* and then renormalized to the heparanase level in the 'whole tumor' sample. As shown in Figure 1c, heparanase expression in RIP1-Tag2 tumors is highest in the Gr-1+/Mac-1+ infiltrating immune cell (IC) fraction, as compared to the endothelial (EC) and tumor cell (TC) fractions.

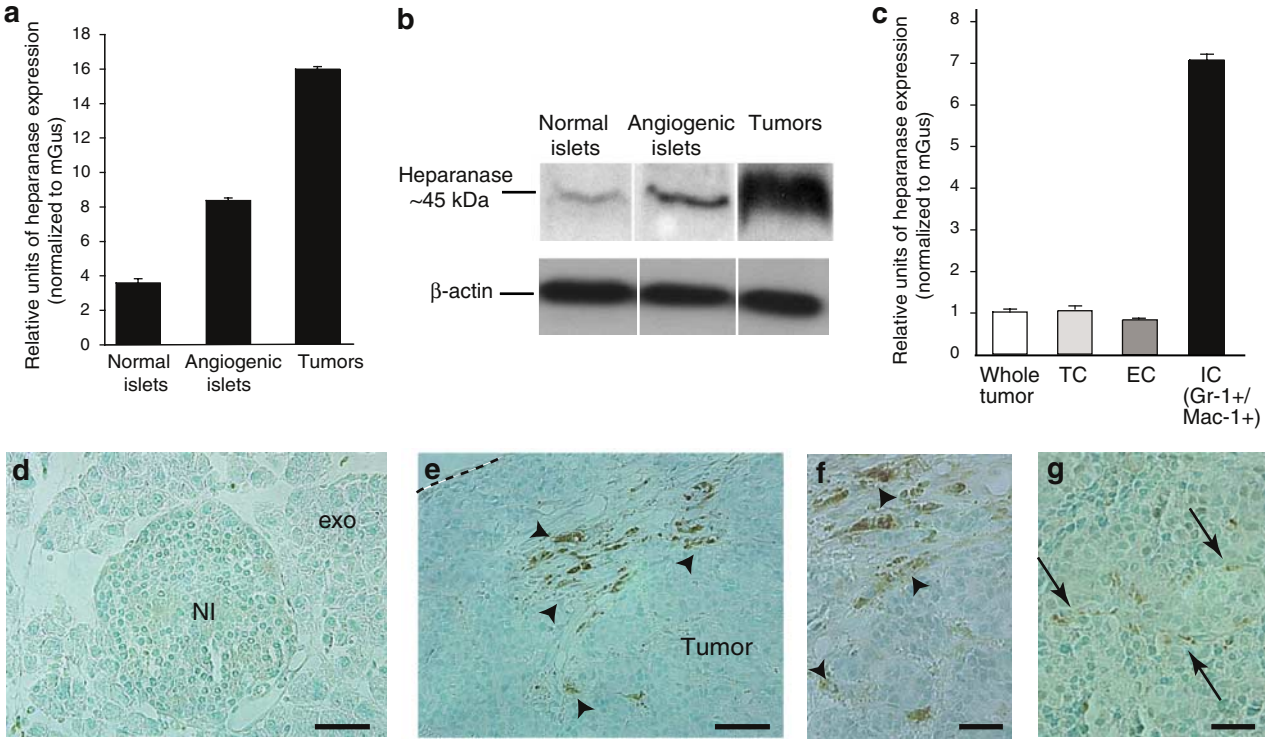

Figure 1 Expression of heparanase mRNA and protein is upregulated during multistage tumorigenesis. (**a**) Real-time quantitative RT–PCR of heparanase in pools of normal islets, angiogenic islets, and tumors from RIP1-Tag2 mice reveals a significant increase in mRNA expression as tumors develop. (**b**) Heparanase protein expression as detected by Western blotting also increases with tumor progression through the same three stages. Reprobing of the same Western blot with β-actin confirmed equal protein loading in all samples. (**c**) The majority of heparanase expression in the tumors is supplied by Gr-1+/Mac-1+ infiltrating immune cells (IC), as revealed by quantitative RT–PCR analysis of FACS-purified cell populations. Relative expression levels of heparanase in each cell type were calculated by normalization to *mGus,* and then renormalized to the heparanase level in the 'whole tumor' sample. Controlling for equal cell number, there is a lesser contribution from endothelial cells (EC) and tumor (Tag+) cells (TC). Immunohistochemical staining of heparanase protein (brown) in RIP1-Tag2 pancreas sections reveals no detectable expression in normal islets (NI) or exocrine pancreas (exo) **(d)**. Heparanase protein can be detected in a subset of cells at the periphery of tumors **(e)**, which may be infiltrating immune cells **(f)** and is also associated with endothelial cells **(g)** in islet tumors. The tumor margin in panel e is outlined by a dashed line. Arrowheads indicate stromal/inflammatory cell staining and arrows indicate endothelial cell staining. The scale bar corresponds to 100 μm in panels d and e and 50 μm in panels f and g. Heparanase immunostaining was performed in five independent experiments on tissue sections from RIP1-Tag2 mice (5, 10, and 13 weeks of age), and representative images are shown

Immunohistochemical detection of heparanase (using an antibody that detects both pro- and active forms of the heparanase enzyme) in the pancreas of RIP1-Tag2 mice also revealed an upregulation in protein expression during tumorigenesis. There was no detectable heparanase immunostaining in the normal islets or exocrine pancreas (Figure 1d). This result suggests that immunostaining is not sensitive enough to detect the very low levels of heparanase mRNA and protein in normal islets observed by the real-time quantitative RT–PCR and Western blot analyses. In islet tumors, heparanase staining was detected at the periphery of tumors in a subset of stromal cells, which we infer from the FACS analysis to be predominantly innate immune cells (Figure 1e and f); endothelial cell-associated heparanase expression is also evident (Figure 1g).

Stage-specific trials with a heparan sulfate mimetic reveal multiple effects on the parameters of islet tumorigenesis

To investigate whether the observed increase in heparanase expression is important for islet tumorigenesis, we sought to interfere with heparanase function. Since a gene knockout of heparanase has not to our knowledge been produced, and is anticipated to be lethal, we chose to use a small molecule inhibitor, named PI-88. This agent was identified as a potent inhibitor both of heparanase activity and of the bioavailability and function of HS-binding proteins (e.g. FGF-1, FGF-2) in an extensive screen of sulfated oligosaccharides (Parish *et al*., 1999). PI-88 acts as a noncleavable structural mimetic of HS, occupying the active site of heparanase, thus inhibiting heparanase cleavage of endogenous HS chains. PI-88 has the additional property of directly binding to heparin-binding regulatory factors (Parish *et al*., 1999; Cochran *et al*., 2003; Francis *et al*., 2003; Khachigian and Parish, 2004), potentially perturbing downstream signaling via their receptors (Ornitz, 2000; Powers *et al*., 2000). Both of these effects appear to be relatively specific, in that related oligosaccharides of different lengths and/or number of sulfated residues were not as potent as PI-88 in inhibiting heparanase activity, angiogenesis, or metastasis (Parish *et al*., 1999), indicating that PI-88's

actions are not simply based on a property common to all sulfated oligosaccharides. Thus, PI-88 is a functionally selective probe of HSPG remodeling, serving both to inhibit an enzyme (heparanase) that cleaves HS side chains and to sequester diffusible HS-binding regulatory proteins released by heparanase action or other means.

We used PI-88 in stage-specific pharmacological trials in the RIP-Tag2 model, assessing its effects (and inferentially the roles of heparanase and HS) on the distinctive and well-characterized parameters of this multistage pathway to pancreatic islet carcinoma.

Angiogenic switching in progenitor lesions RIP1-Tag2 mice were treated with PI-88 at two different doses, 30 or 60 mg/kg/day, in three separate trials that target different stages in tumorigenesis (Bergers *et al*., 1999). In a 5.5 weeks prevention trial (PT), treatment from 5 to 10.5 weeks of age is designed to assess the effects of a test agent on initial angiogenic switching in the normal vasculature of hyperplastic progenitor lesions. Daily injection of PI-88 produced a 34% reduction in the number of angiogenic islets evident at the 10.5 weeks end point, when solid tumors are just forming (Figure 2a). There were indistinguishable effects at the two different doses of PI-88 tested: the lower dose (30 mg/kg/day, $n=24$) produced a 34% reduction in angiogenic islet dysplasias compared to PBS-treated controls ($n=18$, $P<0.0001$), similar to the 35% reduction seen at the higher dose (60 mg/kg/day, $n=6$, $P=0.002$).

Tumor growth In an intervention trial (IT, treatment from 10 to 13.5 weeks of age), designed to interfere with the rapid growth of nascent solid tumors, PI-88 reduced cumulative tumor volume by 66–70% at 13.5 weeks of age, relative to littermate, age-matched, PBS-treated controls (Figure 2b). Again, similar effects were observed with both PI-88 doses: 70% reduction in mice treated with PI-88 at the lower dose (30 mg/kg/day, $n=19$) compared to PBS-treated controls ($n=21$, $P<0.0001$), and a similar 66% reduction at the higher dose (60 mg/kg/day, $n=9$, $P=0.0011$).

In a regression trial (RT, treatment from 12 to 16 weeks of age), intended to test the ability of inhibitors to stabilize or regress large tumors and potentially extend lifespan to a defined end point 4 weeks later, PI-88 produced 'stable disease', in that the tumor volume at the end point was comparable to that in mice at the 12-week-old starting point of the trial (Figure 2b). Given that untreated RIP1-Tag2 mice die at 13–14 weeks of age, there were no age-matched controls for the mice treated with PI-88 for 4 weeks to the defined 16 weeks end point. Therefore, we compared the tumor volumes in 13.5-week-old controls with 16-week-old PI-88-treated mice, revealing a 28% reduction tumor burden in PI-88-treated mice (30 mg/kg/day, $n=16$) compared to PBS-treated controls ($n=21$, $P=0.1010$), and a 45% reduction at the higher dose (60 mg/kg/day, $n=14$, $P=0.0147$). Interestingly, there was a significant difference in efficacy between the two doses of PI-88 at this later 16 weeks time point, where treatment at the higher dose resulted in a more pronounced stabilization of tumor growth. This may simply reflect the much higher levels of

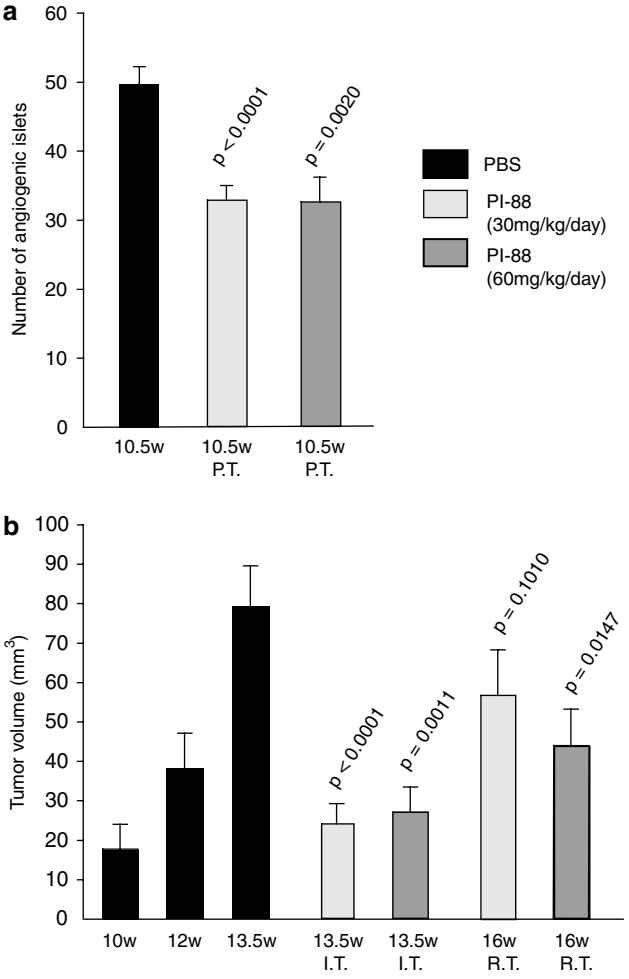

Figure 2 The HS mimetic PI-88 affects angiogenic switching frequency and tumor growth. (**a**) Treatment with PI-88 in a PT (5–10.5 weeks of age) reduces angiogenic switching by 34 and 35% at the lower (30 mg/kg/day; $n=24$) and higher (60 mg/kg/day; $n=6$) doses, respectively, by compared to PBS-treated littermate controls ($n=18$). The number of angiogenic islets was calculated for all groups and the means + s.e.m. are indicated. *P*-values were calculated by comparison of treatment groups to 10.5 weeks controls (Wilcoxon's test). (**b**) PI-88 treatment in the IT (10–13.5 weeks of age) results in a 70 or 66% reduction in cumulative tumor volume at the lower (30 mg/kg/day; $n=19$) and higher (60 mg/kg/day; $n=9$) doses, respectively, compared to PBS-treated littermate controls ($n=21$). In the third RT, PI-88-treated RIP1-Tag2 mice live longer (to the 16 weeks end point) and both dosing regimens essentially stabilize tumor growth, with more pronounced effects at the higher (60 mg/kg/day) dose. There are no age-matched control comparisons for the 16 weeks treated mice, and thus the comparisons were made to 13.5 weeks sham-treated controls. The means + s.e.m. are indicated on the graph. *P*-values were calculated by comparison of both treatment groups to 13.5 weeks controls (Wilcoxon's test)

heparanase protein at these later stages (Figure 1b), requiring higher levels of systemic PI-88 for effective inhibition. The average number of tumors per mouse also decreased significantly following PI-88 treatment. It was observed that 13.5-week-old control RIP1-Tag2 mice had an average tumor number of 10.9 compared to 3.8 for PI-88-treated mice (30 mg/kg/day) at the same age ($P<0.0001$).

To investigate the mechanism(s) underlying the effects of the HS mimetic on these multiple stages of tumor progression, we assessed various cellular parameters of tumorigenesis including cell death, cell proliferation, angiogenesis, and tumor invasion.

Tumor cell proliferation and apoptosis Comparison of the rates of apoptosis, as determined by TUNEL staining, revealed a significant increase in tumor cell death in PI-88-treated *versus* control tumors (Figure 3a–c), by almost threefold in both IT and RT as compared to untreated 13.5 weeks controls ($P=0.0002$ and 0.0029 in PI-88 IT and RT respectively *versus* 13.5 weeks PBS). Moreover, PI-88 treatment decreased the levels of cell proliferation in the same lesions (Figure 3d–f). The percentage of cells in S-phase, as assessed by BrdU incorporation, decreased by 58% in PI-88-treated angiogenic islets compared to 10.5 weeks controls, ($P=0.0021$), and by 52 and 55% in the IT and RT

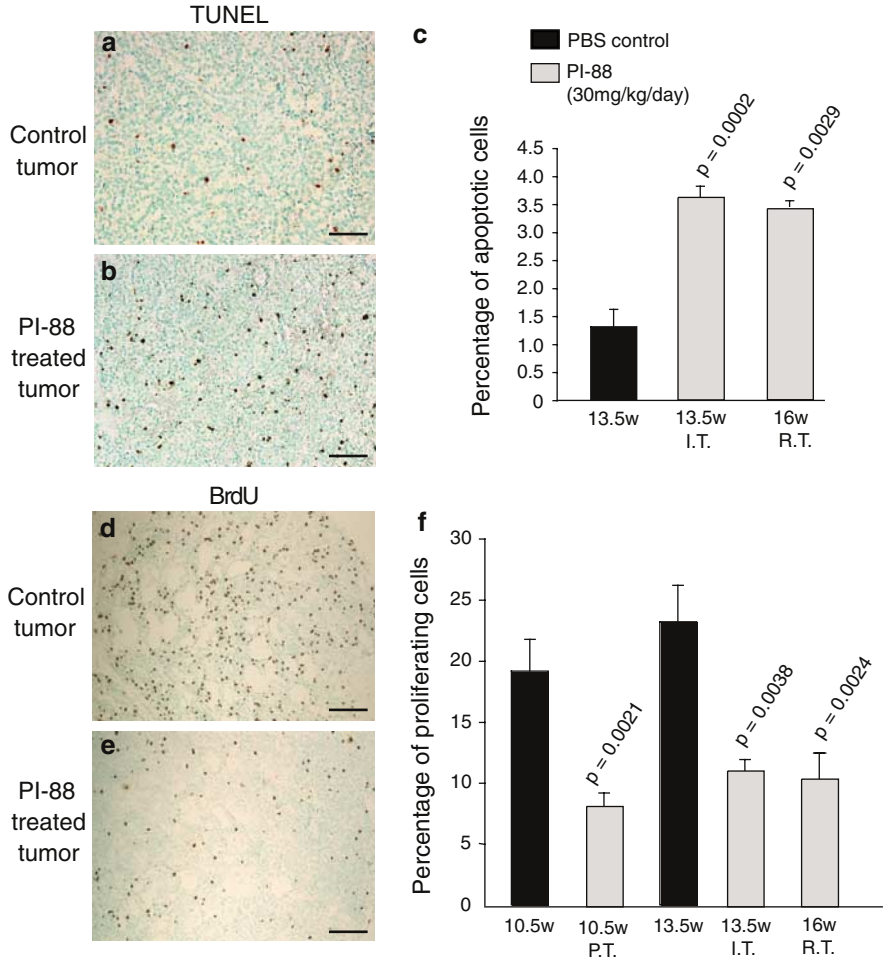

Figure 3 Effects of the HS mimetic PI-88 on tumor cell proliferation and apoptosis. (**a**, **b**) To examine the effects of PI-88 treatment on cell death, control and PI-88-treated tumors were stained for the presence of apoptotic cells by TUNEL. Representative images from control (**a**) and PI-88-treated (**b**) tumors at 13.5 weeks of age are shown. (**c**) Apoptosis was quantitated in tumors from RIP1-Tag2 mice treated with PI-88 in either an IT or RT and compared to control 13.5 weeks tumors. The means + s.e.m. of the percentage of apoptotic cells are indicated on the graph. Apoptosis was increased by 2.8-fold in the IT comparison and 2.5-fold in the RT comparison to controls. *P*-values were calculated by comparison of both treatment groups to 13.5-week sham-treated controls (Wilcoxon test). (**d**, **e**) Effects of PI-88 treatment on cell proliferation, as measured by BrdU staining, were examined in all three PI-88 trials. Representative images from control (**d**) and PI-88 treated (**e**) tumors at 13.5 weeks are shown. (**f**) Cell proliferation was quantitated in angiogenic islets (PT) and in tumors (IT or RT) from mice treated with PI-88, and compared with age-matched control lesions. The means + s.e.m. of the percentage of dividing cells in S-phase are indicated on the graph. Cell proliferation was decreased by 58, 52 and 55% respectively in the PT, IT, and RT comparisons to controls. *P*-values were calculated by comparison of the 10.5 weeks end point treatment group (PT) to 10.5 weeks controls, and the 13.5-week (IT) and 16-week (RT) end point treatment groups to 13.5 weeks controls (Wilcoxon's test). Graphs in panels c and f show the cumulative data obtained from blinded analysis of at least five mice per treatment or control group, with 5–15 independent fields ($\times 200$ magnification) typically counted per mouse. The scale bar corresponds to 100 μm in all panels

respectively compared to untreated 13.5 weeks controls ($P=0.0038$ and 0.0024 in PI-88 IT and RT respectively *versus* 13.5 weeks PBS). This combination, of a significant decrease in cell proliferation and marked increase in cell death presumably accounts for the pronounced reduction in tumor growth observed following PI-88 treatment.

Angiogenesis and the neovasculature To assess the effects, if any, of PI-88 treatment on the vasculature of angiogenic islets and tumors, we perfused treated and control RIP1-Tag2 mice with FITC-lectin to visualize functional blood vessels. Many of the PI-88-treated angiogenic islets showed a decrease in the overall number of blood vessels, as compared to untreated lesions (representative images are shown in Figure 4a and d compared to Figure 4b and e), but other angiogenic islets were only modestly affected (example shown in Figure 4c and f). Similar effects were observed at later stages of treatment, with some tumors showing a dramatic decrease in vascularity (Figure 4g and j: control tumor *versus* Figure 4h and k: PI-88-treated tumor), and other tumors showing modest effects (Figure 4i and l). The number of blood vessels in PI-88-treated angiogenic islets and tumors was quantified and compared to untreated age-matched controls, revealing an average reduction of 73% ($P=0.0002$) in the PT, 72% ($P=0.0002$) in the IT, and 70% ($P<0.0001$) in the RT, respectively (Figure 4m).

To begin elucidating the mechanism underlying these significant effects on tumor angiogenesis following PI-88 treatment, we examined the association of the angiogenic growth factor VEGF-A with its receptor, VEGF-R2, using the GV39M antibody (Brekken *et al*., 1998). This antibody specifically recognizes VEGF-A ligand when bound to its cognate receptor VEGFR-2; this complex is abundant on the angiogenic endothelium of various highly vascularized tumors (Brekken *et al*., 1998; Bergers *et al*., 2000; Rodriguez-Manzaneque *et al*., 2001; Giraudo *et al*., 2004). In normal tissues where VEGF-A is constitutively expressed (such as normal islets (Bergers *et al*., 2000)), the majority of the protein is sequestered in the BM/ECM, likely due to the heparin-binding motifs present in most isoforms, and very little of the VEGF-A/VEGFR2 complex is substantively detectable with GV39M (Bergers *et al*., 2000). In contrast, the bioavailability of the VEGF-A protein to its receptor is increased in many tumors, as evidenced by the angiogenic phenotype of the tumor endothelial cells, and the prevalent staining with GV39M, concomitant with the production of matrix-remodeling enzymes, such as MMP-9 (Bergers *et al*., 2000; Rodriguez-Manzaneque *et al*., 2001; Giraudo *et al*., 2004).

To determine whether inhibition of HS and/or heparanase function was affecting the bioavailability of VEGF-A in tumors, we stained control and PI-88-treated RIP1-Tag2 tumors with the GV39M antibody. In control RIP1-Tag2 tumors, GV39M coats the endothelium, visualized with MECA-32 immunostaining (Figure 5a and c), resulting in a tight colocalization between the two markers (Figure 5e and g). However, in PI-88-treated tumors there is a marked reduction in the overall levels of GV39M staining (Figure 5b, d, f and h), indicating that treatment with the HS mimetic, PI-88, significantly interfered with the formation of the complex between VEGF-A and its receptor VEGF-R2. The percentage of VEGF/VEGF-R2 complex associated with tumor blood vessels was quantitated in PI-88-treated and untreated age-matched control tumors, revealing a 65% decrease in the PI-88-treated tumors ($P=0.0079$) (Figure 5i).

Angiogenesis in this mouse model can also be assessed, and the frequency of angiogenic switching quantitated, *ex vivo* in a collagen gel or 'starburst' angiogenesis bioassay. In this assay, endothelial cells are dispersed in the gel and attracted to a source of pro-angiogenic factors, such as an angiogenic islet or tumor, thus forming tubes in a starburst pattern (Folkman *et al*., 1989). We used this bioassay to further assess the functional involvement of heparanase activity and/or HS-binding protein bioavailability in regulating the angiogenic phenotype that is focally activated in a subset of hyperplastic/dysplastic islets. Angiogenic islets were isolated from 8 to 9 week-old RIP1-Tag2 mice and tested individually *ex vivo* for their ability to attract endothelial cells in the collagen gel assay (Folkman *et al*., 1989; Compagni *et al*., 2000). After 48 h of incubation, angiogenic islets were scored into three categories based on their ability to attract EC tubes, strong, weak, or no response (Compagni *et al*., 2000), with representative images shown in Figure 6a–c. There was a dose-related response when PI-88 was added to the collagen gel, as shown in Figure 6d, indicating a direct inhibition of endothelial migration to the angiogenic islets in the presence of this multifunctional inhibitor. This effect was not due to PI-88 toxicity, as

Figure 4 The angiogenic vasculature is variably reduced in premalignant lesions and tumors by PI-88. RIP1-Tag2 mice were perfused with FITC-lectin to visualize the functional blood vasculature. FITC-lectin-perfused tissues are shown in green in the top panels, with the corresponding image merged with DAPI (blue) to visualize the nuclei in the lower panels. Angiogenic islets from control RIP1-Tag2 mice are highly vascularized (**a**, **d**). In contrast, many of the angiogenic islets in PI-88-treated 10.5-week-old mice show an impaired vasculature, albeit with some variability in effect (**b**, **e** and **c**, **f**). Similarly, at later stages, tumors from control 13.5-week-old RIP1-Tag2 mice show an extensive vascularization (**g**, **j**), whereas the vasculature in many tumors from mice treated with PI-88 is perturbed to varying degrees (**h**, **i** and **k**, **l**). AI indicates angiogenic islets, T indicates tumor tissue, and exo indicates the normal exocrine pancreas. The scale bar corresponds to 100 μm in all panels. At least five graded lesions per mouse and at least 5 mice per age-matched group were assessed in a blinded fashion following FITC-lectin perfusion; representative images are shown. (**m**) Graph showing the quantitation of the number of blood vessels comparing the various control and PI-88-treated lesions. The mean number of blood vessels per $\times 200$ field plus s.e.m. are shown, demonstrating an average reduction of 73% ($P=0.0002$) in the PT, 72% ($P=0.0002$) in the IT, and 70% ($P<0.0001$) in the RT, respectively (**m**)

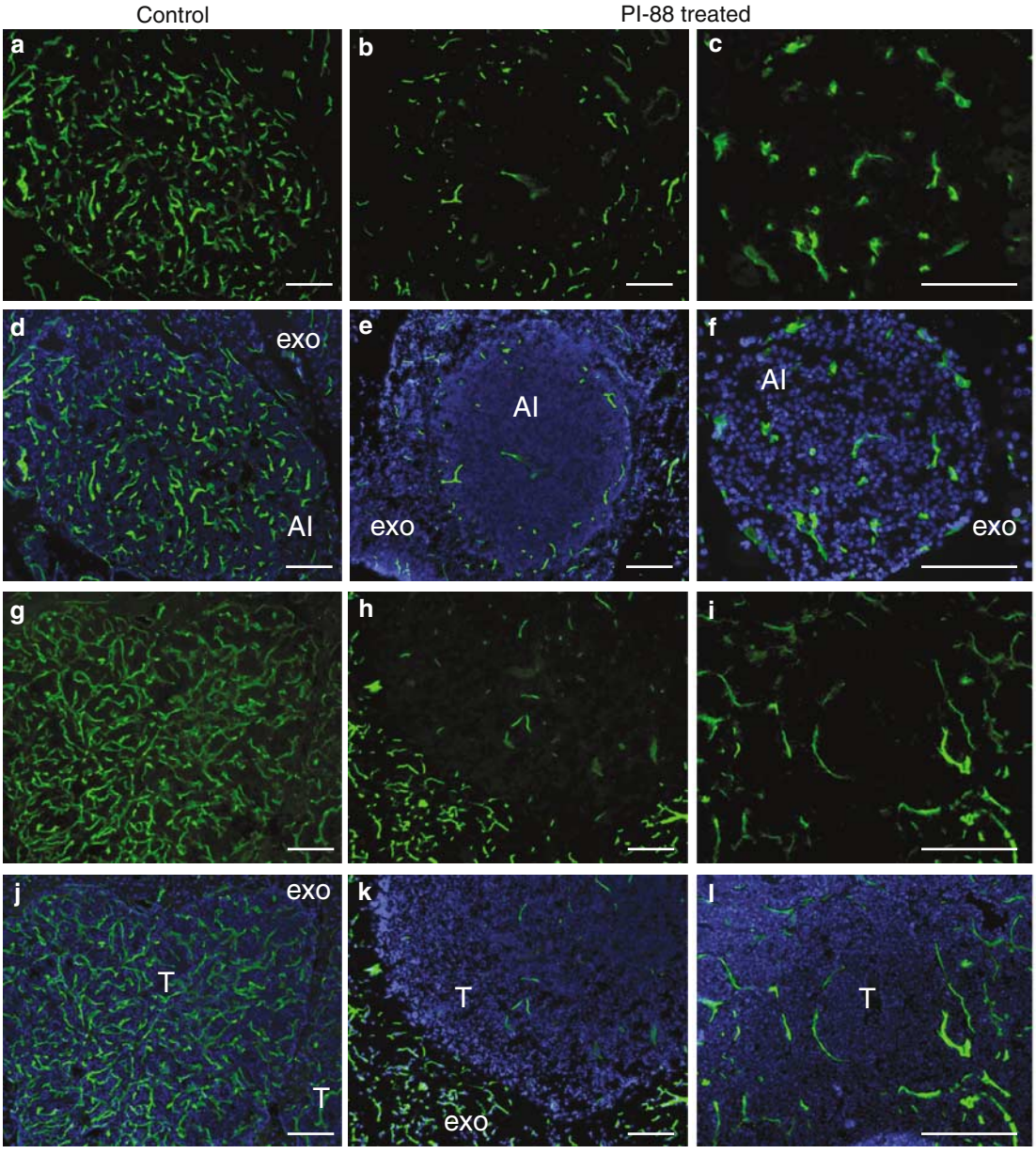
Control
PI-88 treated
a
b
c
d
exo
AI
e
AI
exo
f
AI
exo
g
h
i
j
exo
T
T
k
T
exo
l
T

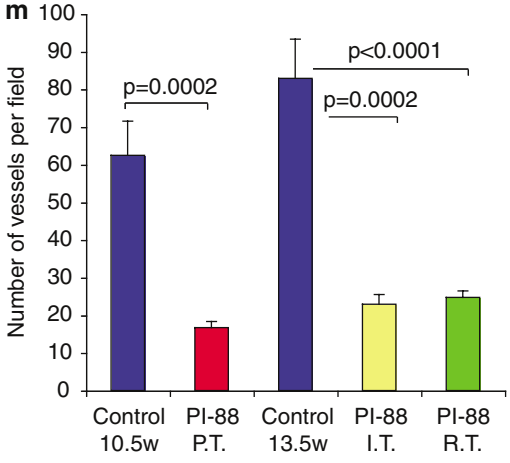
m
Number of vessels per field
100
90
80
70
60
50
40
30
20
10
0
p=0.0002
p<0.0001
p=0.0002
Control 10.5w
PI-88 P.T.
Control 13.5w
PI-88 I.T.
PI-88 R.T.

the endothelial cells were still viable after 48 h of incubation (data not shown). Collectively, the *in vivo* and *ex vivo* data clearly implicate heparanase and/or otherwise mobilized HS-binding regulatory factors, as revealed by PI-88's capability to target both entities, in regulating angiogenesis in neoplastic and malignant lesions of this multistep pathway.

Invasion Progression to an invasive growth capability is a hallmark of malignant progression and a stage

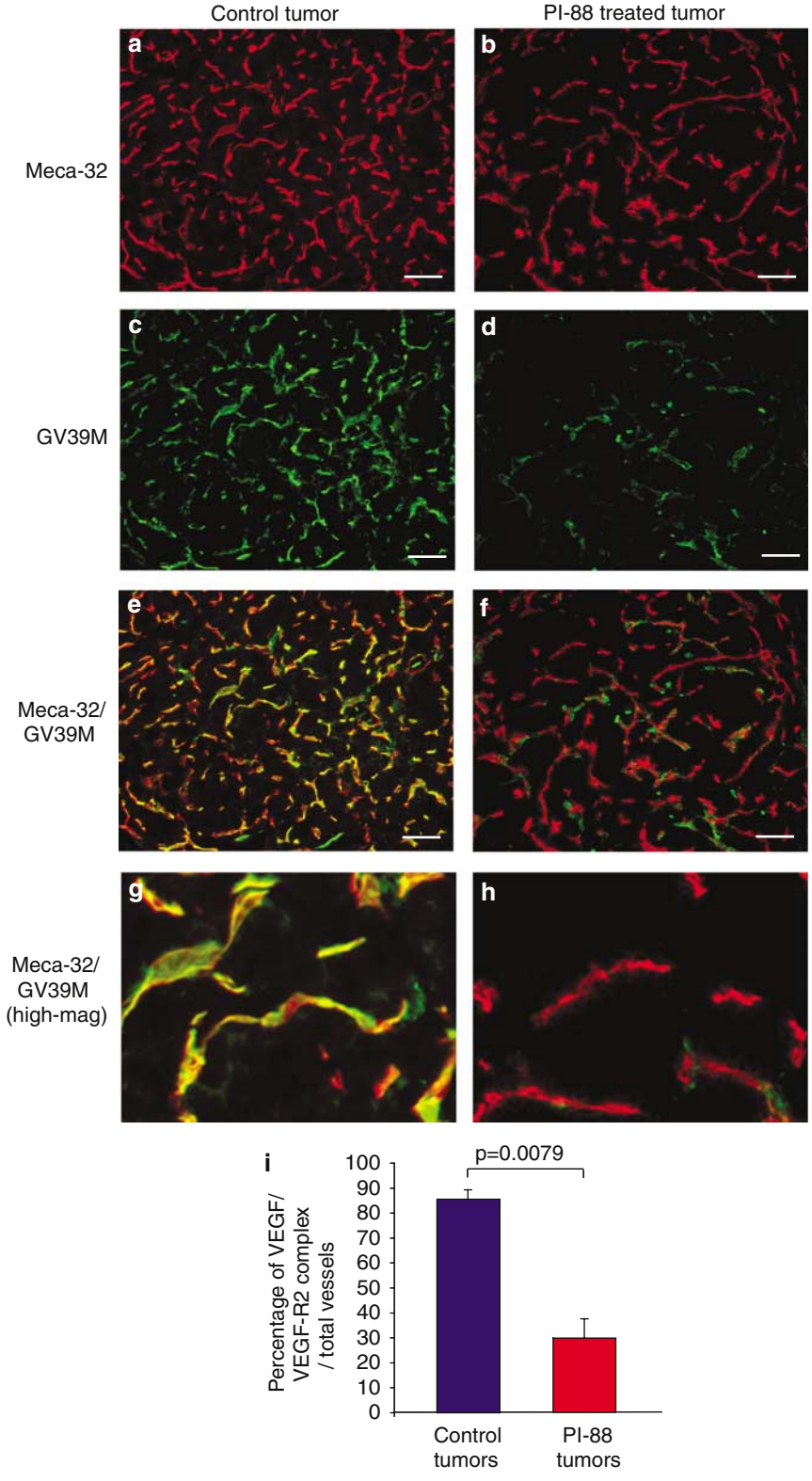

during tumorigenesis in which heparanase activity has been widely implicated from studies on various human cancers. We sought, therefore, to investigate the effects of inhibiting heparanase (and potentially other HS-mediated activities) with PI-88 on tumor invasion in this model of pancreatic neuroendocrine cancer. Treated and control tumors from the IT and RT trials described above were evaluated. Tumors in RIP1-Tag2 mice can be classified into three different grades: adenomatous, often encapsulated tumors with a well-circumscribed margin (Tum), microinvasive carcinomas (IC1), and invasive carcinomas (IC2) (Lopez and Hanahan, 2002). Representative images of the predominant grades in control tumors (IC1) and PI-88-treated tumors (Tum) are shown in Figure 7a and b, and c and d, respectively. Comparison of tumor grades between the groups shows a clear shift towards encapsulated tumors in the IT and RT groups (57 and 80% Tum, respectively), as compared to tumors in control mice at the 12 weeks starting point and 13.5 weeks end stage (32 and 15% Tum, respectively) (Figure 7e). Indeed, the effect on suppression of invasion following PI-88 administration was most pronounced in RT (16 weeks tumors).

To investigate the mechanism by which PI-88 reduced invasion, we used reconstituted basement membrane (Matrigel) invasion assays. We observed a significant dose-dependent reduction in tumor cell invasion when a single-cell suspension of whole RIP1-Tag2 tumors (including Tag+ tumor cells, endothelial and innate immune cells, pericytes, etc.) was presented with a Matrigel barrier in the presence of a chemoattractant (10% serum) with or without added PI-88 (Figure 7f). Interestingly, when we used pure tumor cells in this assay (i.e. cells from the βTC3 tumor cell line derived from an RIP1-Tag2 tumor; Efrat *et al*., 1988), we observed a much reduced invasive capacity, as compared to the whole tumor suspension, and little or no effect of PI-88. This suggests that the overt tumor cells, at least in this assay, require other cell types (found in the whole tumor suspension), presumably providing heparanase and possibly other proinvasive molecules for effective *in vitro* invasion.

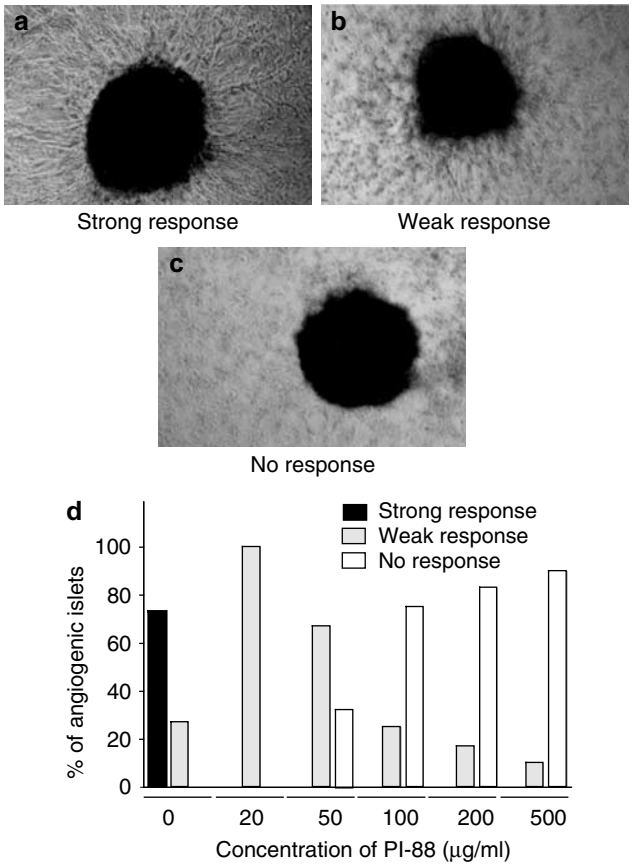

Figure 6 *Ex vivo* angiogenesis in a collagen gel bioassay is inhibited by PI-88. RIP1-Tag2 angiogenic islets were cocultured with endothelial cells in a three-dimensional collagen matrix containing different concentrations of PI-88. Representative examples of a strong response (**a**), a weak response (**b**), and no response (**c**) of endothelial cells to the angiogenic islet in culture are shown. The *ex vivo* angiogenesis assay was performed on five independent occasions, using at least 10 angiogenic islets per experimental group, and the responses scored as above and graphed (**d**)

Discussion

Remodeling of the ECM and BM is critical for processes ranging from normal embryonic development to wound healing and tumorigenesis. During tumor development, this turnover occurs in a highly ordered manner involving the coordinated action of proteases and endoglycosidases. This process not only contributes to angiogenesis and tumor invasion, but also results in the

Figure 5 PI-88 treatment results in reduced VEGF-A bioavailability, as monitored by VEGF-A/VEGF-R2 complex formation. To assess the bioavailability of VEGF-A, control and PI-88-treated tumors were stained with GV39M, an antibody that specifically recognizes VEGF-A when associated with its receptor VEGFR-2. (**a**, **b**) Meca-32 staining was used to visualize the endothelium; representative images from control (**a**) and PI-88-treated (**b**) tumors at 13.5 weeks are shown. (**c**, **d**) GV39M staining was used to detect the VEGF-A/VEGF-R2 complex; representative images from control (**c**) and PI-88-treated (**d**) tumors at 13.5 weeks are shown. (**e**, **f**). The merged image of Meca-32 and GV39M staining reveals abundant colocalization of the two markers in control (**e**) tumors. Notably, there is a marked reduction in both GV39M staining and colocalization with Meca-32, in the PI-88-treated (**f**) tumors. (**g**, **h**). Comparison of Meca-32/GV39M colocalization is shown at higher magnification in the control (**g**) and PI-88-treated (**h**) tumors. The scale bar corresponds to 50 μm in all panels. At least five graded lesions per mouse and at least five mice per age-matched group were stained with the GV39M antibody. (**i**) Graph showing the number of VEGF/VEGF-R2-positive vessels calculated as a percentage of the total number of vessels in control and PI-88-treated tumors. The mean percentage of GV39M-positive blood vessels divided by the total number of blood vessels per $\times 200$ field, plus s.e.m. are shown, demonstrating an average reduction of 65% ($P = 0.0079$)

release of HS-binding proteins such as chemokines and proangiogenic growth factors, thus setting off numerous downstream signaling cascades. While large families of proteases (matrix metalloproteases, aspartic, cysteine, and serine proteases) are responsible for the cleavage of protein components of the BM/ECM, cleavage of the HS side chains is performed by a limited set of enzymes, including an endoglycosidase, heparanase.

Heparanase activity has been implicated in human cancers from a number of descriptive studies on clinical samples, demonstrating a correlation between tumor malignancy and heparanase levels (Nakajima *et al*., 1988; Friedmann *et al*., 2000; Koliopanos *et al*., 2001; Uno *et al*., 2001; Zcharia *et al*., 2001; Kim *et al*., 2002; Maxhimer *et al*., 2002; Tang *et al*., 2002; Kelly *et al*., 2003). In addition, various *in vitro* and *in vivo* studies

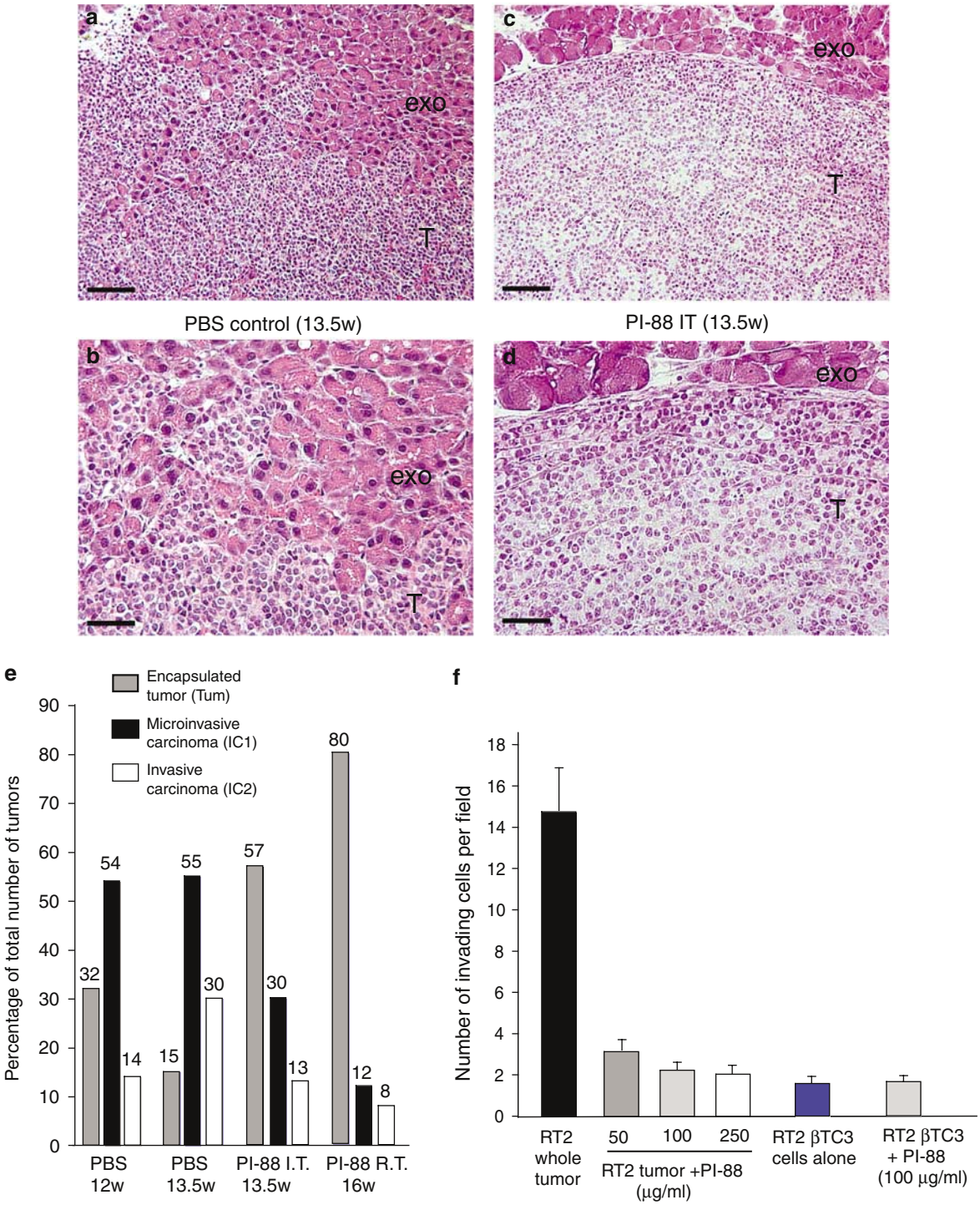

have provided evidence suggestive of a role for heparanase in tumor invasion and metastasis (Hulett *et al*., 1999; Vlodavsky *et al*., 1999; Koliopanos *et al*., 2001; Uno *et al*., 2001; Goldshmidt *et al*., 2002; Kelly *et al*., 2003; Zetser *et al*., 2003); notably, many of these studies have involved overexpressing heparanase in tumor cell lines and inference of its function from what may have been nonphysiological levels of the enzyme. The present study, taking another approach, has found that the endogenous heparanase gene is naturally upregulated at the mRNA and protein levels during multistage tumorigenesis in a well-characterized mouse model of endogenous cancer, in which these sequential stages arise progressively over time and can be clearly identified and studied. By using an inhibitor of heparanase activity, we have further shown that this increase in heparanase during RIP1-Tag2 tumorigenesis serves multiple functions: promoting cell survival, cell proliferation, angiogenesis, and invasion.

Previous *in vitro* studies have implicated heparanase activity in particular steps in the angiogenic process, including degradation of the subendothelial BM and ECM during endothelial cell migration (Bartlett *et al*., 1995) and release of HS-bound angiogenic growth factors sequestered in the BM/ECM (Ishai-Michaeli *et al*., 1990; Vlodavsky *et al*., 1996, 1999; Iozzo and San Antonio, 2001). We now demonstrate that both *ex vivo* and *in vivo* angiogenesis are impaired by PI-88, a heparanase and HS-binding protein inhibitor, in this mouse model. Using an *ex vivo* angiogenesis bioassay, we found that the ability of endothelial cells to migrate toward a proangiogenic source (angiogenic islets) and form tubes was impaired in the presence of PI-88. These angiogenic islets abundantly express a number of HS-binding proangiogenic factors including VEGF family members (Inoue *et al*., 2002), and multiple members of the FGF family (JA Joyce and D Hanahan, unpublished data). We have previously shown that VEGF-A is sequestered in normal pancreatic islets, such that it is not bioavailable to its receptor on islet endothelial cells, in a manner whereby it can be released by *ex vivo* incubation with MMP-9 (Bergers *et al*., 2000). *In vivo*, VEGF mobilization occurs concomitant with the angiogenic switch and with the appearance of MMP-9 activity (Bergers *et al*., 2000). We now show that VEGF mobilization (as monitored by the association of VEGF-A with its receptor VEGFR-2) is greatly reduced in tumors following treatment with the HS mimetic PI-88. This result suggests that heparanase is also involved in mobilizing VEGF-A from its sequestered configuration in normal islets. By analogy, other ECM-sequestered (heparin-binding) growth factors could be similarly activated to participate in angiogenesis or other aspects of tumor growth and progression.

PI-88, however, has a second function, since in addition to inhibiting heparanase activity, this HS mimic can directly bind to HS-binding proteins, thereby impairing their function (Parish *et al*., 1999; Cochran *et al*., 2003; Francis *et al*., 2003; Khachigian and Parish, 2004). Thus, the angiogenesis inhibition that we observe *in vivo* may reflect both of these mechanisms, each serving the same outcome: namely, to limit the bioavailability of HS-binding growth factors. Similarly, the significant effects on apoptosis and proliferation following systemic PI-88 administration may result from either direct trapping of soluble growth and survival factors or inhibition of heparanase-mediated release of such proteins sequestered in the ECM. More specific heparanase inhibitors (e.g. neutralizing antibodies; Levidiotis *et al*., 2004) or a conditional gene knockout of the heparanase gene should enable the relative importance of these mechanisms to be discerned.

PI-88 significantly reduced the rate of progression to invasive carcinoma, consistent with prior reports of an association between heparanase expression and/or activity and invasiveness. To our knowledge, this is the first study showing that inhibition of the enzyme produced solely by the endogenous heparanase gene *in vivo* significantly reduces tumor invasiveness. We observed a significant shift from invasive carcinomas to less aggressive, encapsulated tumors following PI-88 treatment, correlating with increased collagen-I deposition, both interstitially and particularly in the tumor capsule (data not shown).

A note of caution could be raised with regard to the therapeutic use of sulfated oligosaccharides in general and PI-88 in particular, in that a large body of literature has documented the capability of heparin and other sulfated oligosaccharides to facilitate (as opposed to inhibit) growth factor signaling. While the weight of evidence indicates that PI-88 is distinct from sulfated oligosaccharides in general (Parish *et al*., 1999) in its

Figure 7 The HS mimetic PI-88 inhibits tumor cell invasion *in vivo* and *in vitro*. (**a**–**d**) Tumor grading of control and treatment groups revealed that the majority of control tumors fall into the invasive carcinoma classes (IC1/2), as illustrated in a representative image (**a**) with higher magnification to show the invasive edges in (**b**), and quantitated in (**e**). In contrast, the majority of PI-88-treated tumors are in the benign, encapsulated Tum class (**c**), with higher magnification of the same representative tumor (**d**) showing the intact tumor capsule, and quantitated in (**e**). The scale bar corresponds to 100 μm in (**a**, **b**) and 50 μm in (**c**, **d**). (**e**) Graph showing the relative proportions of encapsulated (Tum), microinvasive (IC1), and highly invasive carcinomas (IC2) in 12- and 13.5 weeks controls compared to 13.5 weeks (IT) and 16 weeks (RT) PI-88-treated mice, revealing fewer malignant tumors following PI-88 treatment. For grading of tumors, paraffin or frozen tissue blocks were sectioned completely and tissue sections were stained by hematoxylin and eosin every 50 μM. All tumors in all treated and control RIP1-Tag2 mice were graded blindly and subsequently decoded. (**f**) Graph showing that *in vitro* invasion of a single-cell suspension of whole RIP1-Tag2 tumors (containing infiltrating immune cells, endothelial cells, and pericytes in addition to tumor cells) through Matrigel-coated wells in response to a chemoattractant (10% serum) is impaired when PI-88 is included at different concentrations in the incubation media. The assay was also performed in parallel using tumor cells alone, in which the same number of βTC3 cells (clonally derived from an RIP1-Tag2 tumor) were allowed to invade through Matrigel, under the same conditions as the whole tumor suspension, revealing a much lower invasive capacity, irrespective of whether PI-88 was in the incubation media or not. The invasion assay was repeated in five separate experiments, with all control and experimental groups performed in parallel

selective capability to inhibit heparanase, angiogenesis, and metastasis, one cannot exclude the possibility that in certain special situations, it might actually promote growth factor signaling, by virtue of its core polysaccharide motif. Notably, when the correlation between oligosaccharide length and growth factor signaling was examined, heparin fragments of 16–18 sugar units were found to inhibit the binding of VEGF-165 to VEGF receptors, whereas fragments larger than 22 sugar units potentiated the binding (Soker *et al*., 1994). PI-88 is a tetra/pentasaccharide. In one recent study, PI-88 was observed to enhance release of the HS-binding growth factor FGF-2, and yet PI-88 inhibited FGF2-mediated cell signaling, presumably by binding to the soluble growth factor and thereby blocking receptor binding (Francis *et al*., 2003). We have seen no indications of tumor-promoting activity in the RIP1-Tag2 trials; rather, the data are consistent with PI-88 acting to inhibit heparanase and HS effector functions, with the consequent antiangiogenic and antiinvasive effects, and therapeutic efficacy.

Multiplex involvement of degradative enzymes in islet tumorigenesis

It is pertinent to consider these results in the context of previous studies in this mouse model that have documented the upregulation and functional contributions of other enzymes to tumorigenesis of the pancreatic islets. Two matrix metalloproteinases, MMP-9 and MMP-2, are upregulated (Bergers *et al*., 2000), as are six cysteine cathepsin proteases (Joyce *et al*., 2004). Infiltrating innate immune cells are implicated as a prominent source of both classes of proteases, much as we infer for heparanase. MMP gene knockout mice and pharmacological inhibitors of MMP-9 and MMP-2 have collectively demonstrated that MMP-9 is involved both in initial angiogenic switching in hyperplastic islets and subsequent tumor angiogenesis and tumor growth, whereas MMP-2 affected only the tumor stages; remarkably, neither gene knockout nor MMP inhibitors indicated a role for either in the frequent progression to invasive carcinoma (Bergers *et al*., 2000). A broad-spectrum cathepsin protease inhibitor also impaired angiogenic switching and tumor growth, but in addition suppressed invasiveness (Joyce *et al*., 2004), much like PI-88.

How is it that all three of these enzyme classes are affecting angiogenic switching and tumor growth, and two (cathepsins and heparanase) are similarly impairing invasion? One hypothesis is that each class acts in parallel pathways, since none of the class-specific inhibitors completely abrogated a particular function ('the redundancy hypothesis'). Another hypothesis would place these enzymes at different points in the same regulatory pathways for angiogenesis, invasion, etc. Combinatorial therapeutic trials may shed light on these alternative hypotheses. In preliminary studies, we found no additive benefit of combining an MMP inhibitor with PI-88 (JA Joyce and D Hanahan, unpublished data), suggesting that the MMPs and heparanase act in the same pathway to regulate angiogenesis and tumor growth. Similar trials combining PI-88 with cathepsin inhibitors may reveal distinctive or overlapping effects on these phenotypes as well as on invasive growth, to which both cathepsins and heparanase contribute. In addition to these functional studies, it will be important to further delineate the nature of the innate immune cell types that infiltrate neoplastic lesions in this model and deliver these proangiogenic and proinvasive enzymes, to ascertain whether the same cells (and cell types) express all three enzyme classes in the various stages of tumorigenesis, and to determine how the infiltrating immune cells are regulated in terms of their recruitment and their expression of these enzymes.

In conclusion, this study has shown that heparanase is upregulated in a mouse model of multistage carcinogenesis, much as it is in a variety of human cancers. By using a multifunctional inhibitor, we have clearly implicated heparanase and the HSPG network in the regulation of multiple capabilities crucial for tumor growth and progression. The results thus encourage ongoing clinical evaluation of PI-88, and predict that it and perhaps other agents that simultaneously target heparanase and the HS-binding proteins it liberates will prove to have efficacy when appropriately used as therapeutic modalities against a range of human cancers.

Materials and methods

PI-88 preparation

PI-88, provided by Progen Industries Limited (Brisbane, Australia), was prepared as previously described (Parish *et al*., 1999; Ferro *et al*., 2001) by the sulfation of phosphomanno-oligosaccharides derived from the phosphomannan produced by the yeast *Pichia holsti*. It consists predominantly of sulfated phosphomannopentaose and phosphomannotetraose with its components having a molecular mass range of $\sim$1400 to $\sim$3100 Da.

Animal studies

The generation of RIP1-Tag2 mice as a model of pancreatic islet cell carcinogenesis has been previously reported (Hanahan, 1985). Three different RIP1-Tag2 trials were performed as follows: PT (treatment from 5 to 10.5 weeks of age), IT (treatment from 10 to 13.5 weeks of age), and RT (treatment from 12 to 16 weeks of age). Equal numbers of RIP1-Tag2 males and females were used for each trial, with age-matched littermates used as controls for all trials. PI-88 was solubilized in PBS and administered in a single dose per day subcutaneously in two treatment groups per trial, at either 30 or 60 mg/kg/day. Control RIP1-Tag2 littermate animals were treated with a single dose of PBS subcutaneously every day. Tumor volume and angiogenic islet quantitation were performed as described previously (Inoue *et al*., 2002; Bergers *et al*., 2003), and the Wilcoxon's t-test was used for statistical analyses and calculation of means and s.e.m. All animal studies were performed using protocols approved by the animal care and utilization committee at the University of California at San Francisco.

Real-time quantitative PCR

Normal (nontransgenic BL/6) islets were collected as described previously (Parangi *et al*., 1995). Angiogenic islets were isolated from 8-week-old RIP1-Tag2 mice by collagenase digestion of the excised pancreas, and selected based on their red, hemorrhagic appearance (Parangi *et al*., 1995). Tumors were microdissected from the excised pancreas of 13-week-old RIP1-Tag2 mice and the surrounding exocrine tissue carefully removed. RNA was prepared from pools of snap-frozen islets and tumors using an RNeasy kit (Qiagen, Valencia, CA, USA) and DNAse treated. A 1 μg portion of total RNA from pools of normal, angiogenic islets, or tumors was used to synthesize cDNA using the Superscript II Reverse Transcriptase system (Invitrogen, Carlsbad, CA, USA). Real-time quantitative RT–PCR was performed on cDNA synthesized from these pooled stages using the 5′ nuclease assay (real-time TaqMan RT–PCR) with the ABI PRISM 7700 instrument as previously described (Elson *et al*., 2001). Gene-specific primers and probes were designed for heparanase (forward primer: 5′-TGGTTGGGAGAGACGAGCTC-3′; reverse primer: 5′-AGTGGTAGTTGCCTGCTCCG-3′; TaqMan probe (5′–3′): TGCAGCTGGCTTTATGTGGCTGGATAA) and for beta-glucuronidase (*mGus*) (D'Amore *et al*., 1988) (forward primer 5′-CTCATCTGGAATTTCGCCGA-3′; reverse primer; 5′-GGCGAGTGAAGATCCCCTTC-3′; TaqMan probe (5′–3′): CGAACCAGTCACCGCTGAGAGTAATCG).

Flow cytometry

Tumors were excised from 13 to 14 week-old RIP1-Tag2 mice and inflammatory (Mac-1 + /Gr-1 +), endothelial (CD-31 +), and tumor cells collected as described previously (Bergers *et al*., 2003). Briefly, mice were killed and tumors excised from the pancreas and all exocrine tissue was carefully removed. Pools of tumors were minced with a razor blade on ice in 1 × PBS. The minced tumor fragments were then digested at 37°C for 13 min with a collagenase solution containing 0.2 g BSA (Sigma Aldrich, St Louis, MO, USA), 0.05 g collagenase II, 0.05 g collagenase IV and 0.02 g DNase I (all from Worthington Biochemical Corp., Lakewood, NJ, USA), and passed through a 70 μm cell strainer. The tumor cells were washed, the red blood cells lysed with PharM Lyse (BD PharMingen) for 15 s, and then washed again. The cell pellets were resuspended in FACS buffer (1 × PBS/1% BSA), preblocked with an Fc block (CD16/CD32; BD PharMingen), and then incubated with primary antibodies on ice for 30 min: CD31-PE, 1 : 100 (recognizing the CD-31 antigen on endothelial cells); Ly-6G, 1 : 60 (recognizing the GR-1 antigen on granulocytes), from BD PharMingen; CD11b, 1 : 40 (recognizing the Mac-1 antigen on macrophages and other immune cell types) from BD PharMingen. The cells were washed and Via-Probe was added as a cell death indicator (BD PharMingen). The cells were then sorted on a FACSVantage SE flow cytometer using the Cell Quest Pro software version 4 from Becton Dickinson Immunocytometry Systems (Franklin Lakes, NJ, USA). The FL2 gate identified the CD31 + cells, the FL1 gate identified the Gr-1 + /Mac-1 + cells, and the FL3 gate excluded the dead cells.

Histology and immunohistochemistry

Immunohistochemical staining of heparanase protein was performed using a rabbit anti-mouse antibody. New Zealand white rabbits were immunized with a synthetic murine heparanase peptide (KHLKVPPPLFRKPVDT, amino acids 455–470) (Hulett *et al*., 1999) that was coupled to keyhole limpet hemocyanin (Pierce, Rockford, IL, USA). The anti-heparanase polyclonal antibody was affinity purified by passing the serum from immunized rabbits through a column containing the peptide linked to a Sulfolink gel support (Pierce) and eluting with 100 mM glycine-HCl (pH 2.3) followed by neutralization with 1 M Tris-HCl (pH 7.0). Paraffin sections from 10- and 13-week-old RIP1-Tag2 mice were deparaffinized using standard procedures, and endogenous peroxidase activity was blocked by incubation in 2.5% hydrogen peroxidase in methanol for 20 min at room temperature. Slides were washed in PBS several times and antigen retrieval was performed by microwaving the slides in antigen retrieval citrate buffer (BioGenex, San Ramon, CA, USA) for 10 min on high power, followed by 10 min on low power. Slides were left to cool in the antigen retrieval buffer for 30 min, washed several times in PBS, and tissue sections were pre-incubated with serum-free protein block (DAKO Corporation, Carpinteria, CA, USA) for 15 min, washed in PBS, and then incubated in blocking reagent (1 × PNB; Perkin Elmer Life Sciences, Boston, MA, USA) for 1 h at room temperature. The rabbit anti-mouse heparanase antibody (1 : 500 dilution in 0.5 × PNB reagent) was applied to the sections and incubated at 4°C overnight. Tissue sections were then washed several times in PBS, and incubated with a biotinylated goat anti-rabbit secondary antibody (Jackson ImmunoResearch Laboratories, West Grove, PA, USA; 1 : 200 dilution) for 1 h at room temperature. Following several PBS washes, sections were incubated with the Elite Vectastain ABC kit (Vector Laboratories, Burlingame, CA, USA) for 30 min at room temperature, washed in PBS, and the antibody signal was detected using 3,3′-diaminobenzidine (DAB) peroxidase substrate (Sigma Fast 3,3′-diaminobenzidine tablets, Sigma-Aldrich, St Louis, MO, USA). Tissue sections were counterstained in 1% methyl green solution, washed in isobutanol followed by xylene, and mounted in Cytoseal mounting medium (Richard Allen Scientific, Kalamazoo, MI, USA).

FITC-lectin perfusion to visualize the vasculature was performed as previously described (Inoue *et al*., 2002). Briefly mice were anesthetized, injected intravenously with 50 μg of FITC-labeled lectin (*Lycopersicon esculentum*, Vector Laboratories, Burlingame, CA, USA), which was allowed to circulate for 10 min, followed by heart perfusion with 10% zinc-buffered formalin (Medical Chemical Corp., Torrance, CA, USA). The pancreas was removed, processed through 30% sucrose, and then embedded in Tissue-Tek OCT freezing medium (Sakura Finetek USA, Torrance, CA). Sections (35 μm) were cut and lectin staining was visualized using a Zeiss Axioscope fluorescence microscope. At least five graded lesions per mouse and at least five mice per age-matched group were assessed by FITC-lectin perfusion.

TUNEL staining for apoptotic cells and BrdU staining for proliferating cells in S phase were performed on both paraffin-embedded and frozen sections as described previously (Lopez and Hanahan, 2002). For TUNEL and BrdU quantitation, at least five graded lesions per mouse (typically 10–15) and at least five mice per age-matched group were counted blindly, subsequently decoded, and statistical analysis performed. Immunohistochemical detection of the VEGF/VEGF-R2 complex was performed using the GV39M antibody (Brekken *et al*., 1998) (a kind gift from Dr Rolf Brekken) as previously described (Bergers *et al*., 2000; Giraudo *et al*., 2004). At least five lesions per mouse and at least five mice per age-matched group were stained with the GV39M antibody.

For grading of tumors, paraffin or frozen tissue blocks were sectioned completely and tissue sections were stained by hematoxylin and eosin every 50 μM. All tumors in all treated and control RIP1-Tag2 mice were graded blindly according to previously described parameters (Lopez and Hanahan, 2002), and subsequently decoded.

Western blotting

Protein lysates were prepared from pools of normal islets, angiogenic islets, and tumors, according to standard protocols. A 25 μg portion of each protein lysate was separated by gel electrophoresis on a 10% acrylamide gel. Western blot analysis, using standard protocols, was performed with the anti-heparanase antibody (1 : 1000 dilution). The blots were stripped and reprobed with an anti-β-actin antibody (Sigma) (1 : 10 000 dilution) to confirm equal protein loading.

Cell culture

Primary bovine capillary endothelial cells (generously supplied by K Butterfield and J Folkman, Harvard Medical School, MA, USA) were cultured in DMEM (high-glucose DMEM, Life Technologies, Gaithersburg, MD, USA) supplemented with 10% FCS (HyClone, VWR International, Brisbane, CA, USA), FGF2 (3.0 ng/ml; Life Technologies), 2 mM glutamine (Life Technologies), and penicillin/streptomycin (Life Technologies) in 10% CO_2, at 37°C, in flasks precoated with 1.5% gelatin.

Ex vivo *collagen gel angiogenesis assay*

Angiogenic islets were isolated from 9- to 10-week-old RIP1-Tag2 transgenic mice as described previously (Parangi *et al*., 1995). Bovine endothelial cells were trypsinized, resuspended in 10% FCS/DMEM and cocultured with angiogenic islets in collagen matrix (Vitrogen 100, Cohesion, Palo Alto, CA, USA) as described previously (Folkman *et al*., 1989). After 48 h, the response of endothelial cells to the angiogenic tumor stages was scored as strong, weak, or no response (Compagni *et al*., 2000). The experiment was performed five times with approximately 10–20 islets for each treatment group. PI-88 was dissolved in PBS and added to both the collagen matrix and overlying media in the following concentrations; 20, 50, 100, 200, and 500 μg/ml.

In vitro *Matrigel invasion assay*

Pools of tumors were dissected from 13-week-old RIP1-Tag2 mice, minced, and homogenized to a single cell suspension in serum-free DMEM media. A 300 μl portion of the whole tumor cell suspension (1.0×10^6 cells/ml, containing tumor cells, endothelial cells, pericytes, innate immune cells, etc.) from the homogenized tumors was placed on individual rehydrated ECMatrix inserts (Cell Invasion Assay, ECM 550, Chemicon International, Temecula, CA, USA) overlying DMEM media containing 10% fetal bovine serum that acts as a chemoattractant. PI-88 was dissolved in PBS and added to both the tumor cell suspension and underlying media in the following concentrations; 50, 100, and 250 μg/ml. For the assessment of βTC3 tumor cell invasion, 1.0×10^6 cells/ml were subjected to the same conditions as the whole tumor cell suspension. ECMatrix inserts were incubated for 48 h in a tissue culture incubator at 37°C in 5% CO_2 to allow tumor cell invasion through the matrix. Inserts were removed from the tissue culture plates, wiped with a cotton swab to remove the noninvading cells in the upper part of the chamber, followed by cell staining of the invading cells on the lower part of the chamber. The inserts were removed from the chambers and invading cells counted per $\times 40$ field using a Zeiss upright microscope. The invasion assay was repeated in five separate experiments, with all control and experimental groups performed in parallel.

Acknowledgements

We thank Progen Industries, Australia, for supplying PI-88, and B Creese and D Podger, Progen, Australia, for helpful advice. We thank C Concengco and E Solliven for excellent technical assistance, and D Ginzinger and M Yu, UCSF Cancer Center Genome Facility, for Taqman analysis. We are grateful to K Butterfield and J Folkman, Harvard Medical School, MA, USA, for providing primary bovine endothelial cells, and R Brekken, Hope Heart Institute, WA, USA, for providing the GV39M antibody. We thank Z Werb and O Stevaux for insightful review of the manuscript. JAJ is a Fellow of the Leukemia and Lymphoma Society. This work was supported by the William K Bowes Jr Foundation, the American Cancer Society, and the US National Cancer Institute (DH). CF and CRP are recipients of an Australian National Health and Medical Research Council Program grant.

References

Bartlett MR, Cowden WB and Parish CR. (1995). *J. Leukoc. Biol.*, **57,** 207–213.

Bergers G, Brekken R, McMahon G, Vu TH, Itoh T, Tamaki K, Tanzawa K, Thorpe P, Itohara S, Werb Z and Hanahan D. (2000). *Nat. Cell Biol.*, **2,** 737–744.

Bergers G, Javaherian K, Lo KM, Folkman J and Hanahan D. (1999). *Science*, **284,** 808–812.

Bergers G, Song S, Meyer-Morse N, Bergsland E and Hanahan D. (2003). *J. Clin. Invest.*, **111,** 1287–1295.

Bernfield M, Gotte M, Park PW, Reizes O, Fitzgerald ML, Lincecum J and Zako M. (1999). *Annu. Rev. Biochem.*, **68,** 729–777.

Brekken RA, Huang X, King SW and Thorpe PE. (1998). *Cancer Res.*, **58,** 1952–1959.

Cochran S, Li C, Fairweather JK, Kett WC, Coombe DR and Ferro V. (2003). *J. Med. Chem.*, **46,** 4601–4608.

Compagni A, Wilgenbus P, Impagnatiello MA, Cotten M and Christofori G. (2000). *Cancer Res.*, **60,** 7163–7169.

D'Amore MA, Gallagher PM, Korfhagen TR and Ganschow RE. (1988). *Biochemistry*, **27,** 7131–7140.

Dempsey LA, Plummer TB, Coombes SL and Platt JL. (2000). *Glycobiology*, **10,** 467–475.

Efrat S, Linde S, Kofod H, Spector D, Delannoy M, Grant S, Hanahan D and Baekkeskov S. (1988). *Proc. Natl. Acad. Sci. USA*, **85,** 9037–9041.

Elson DA, Thurston G, Huang LE, Ginzinger DG, McDonald DM, Johnson RS and Arbeit JM. (2001). *Genes Dev.*, **15,** 2520–2532.

Ferro V, Fewings K, Palermo MC and Li C. (2001). *Carbohydrate Res.*, **332,** 183–189.

Folkman J, Watson K, Ingber D and Hanahan D. (1989). *Nature*, **339,** 58–61.

Francis DJ, Parish CR, McGarry M, Santiago FS, Lowe HC, Brown KJ, Bingley JA, Hayward IP, Cowden WB, Campbell JH, Campbell GR, Chesterman CN and Khachigian LM. (2003). *Circ. Res.*, **92,** e70–e77.

Freeman C and Parish CR. (1997). *Biochem. J.*, **325** (Part 1), 229–237.

Freeman C and Parish CR. (1998). *Biochem. J.*, **330** (Part 3), 1341–1350.

Friedmann Y, Vlodavsky I, Aingorn H, Aviv A, Peretz T, Pecker I and Pappo O. (2000). *Am. J. Pathol.*, **157,** 1167–1175.

Giraudo E, Inoue M and Hanahan D. (2004). *J. Clin. Invest.*, **114,** 623–633.

Goldshmidt O, Zcharia E, Abramovitch R, Metzger S, Aingorn H, Friedmann Y, Schirrmacher V, Mitrani E and Vlodavsky I. (2002). *Proc. Natl. Acad. Sci. USA*, **99,** 10031–10036.

Haimov-Kochman R, Friedmann Y, Prus D, Goldman-Wohl DS, Greenfield C, Anteby EY, Aviv A, Vlodavsky I and Yagel S. (2002). *Mol. Hum. Reprod.*, **8,** 566–573.

Hanahan D. (1985). *Nature*, **315,** 115–122.

Hileman RE, Fromm JR, Weiler JM and Linhardt RJ. (1998). *BioEssays*, **20,** 156–167.

Hulett MD, Freeman C, Hamdorf BJ, Baker RT, Harris MJ and Parish CR. (1999). *Nat. Med.*, **5,** 803–809.

Inoue M, Hager JH, Ferrara N, Gerber HP and Hanahan D. (2002). *Cancer Cell.*, **1,** 193–202.

Iozzo RV and San Antonio JD. (2001). *J. Clin. Invest.*, **108,** 349–355.

Ishai-Michaeli R, Eldor A and Vlodavsky I. (1990). *Cell Regul.*, **1,** 833–842.

Joyce JA, Baruch A, Chehade K, Meyer-Morse N, Giraudo E, Tsai FY, Greenbaum DC, Hager JH, Bogyo M and Hanahan D. (2004). *Cancer Cell.*, **5,** 443–453.

Kalluri R. (2003). *Nat. Rev. Cancer*, **3,** 422–433.

Kelly T, Miao HQ, Yang Y, Navarro E, Kussie P, Huang Y, MacLeod V, Casciano J, Joseph L, Zhan F, Zangari M, Barlogie B, Shaughnessy J and Sanderson RD. (2003). *Cancer Res.*, **63,** 8749–8756.

Khachigian LM and Parish CR. (2004). *Cardiovasc. Drug Rev.*, **22,** 1–6.

Kim AW, Xu X, Hollinger EF, Gattuso P, Godellas CV and Prinz RA. (2002). *J. Gastrointest. Surg.*, **6,** 167–172.

Koliopanos A, Friess H, Kleeff J, Shi X, Liao Q, Pecker I, Vlodavsky I, Zimmermann A and Buchler MW. (2001). *Cancer Res.*, **61,** 4655–4659.

Levidiotis V, Freeman C, Tikellis C, Cooper ME and Power DA. (2004). *J. Am. Soc. Nephrol.*, **15,** 68–78.

Lopez T and Hanahan D. (2002). *Cancer Cell*, **1,** 339–353.

Marchetti D, Li J and Shen R. (2000). *Cancer Res.*, **60,** 4767–4770.

Marchetti D and Nicolson GL. (1997). *Adv. Enzyme. Regul.*, **37,** 111–134.

Maxhimer JB, Quiros RM, Stewart R, Dowlatshahi K, Gattuso P, Fan M, Prinz RA and Xu X. (2002). *Surgery*, **132,** 326–333.

Nakajima M, Irimura T and Nicolson GL. (1988). *J. Cell. Biochem.*, **36,** 157–167.

Ornitz DM. (2000). *BioEssays*, **22,** 108–112.

Parangi S, Dietrich W, Christofori G, Lander ES and Hanahan D. (1995). *Cancer Res.*, **55,** 6071–6076.

Parish CR, Freeman C, Brown KJ, Francis DJ and Cowden WB. (1999). *Cancer Res.*, **59,** 3433–3441.

Parish CR, Freeman C and Hulett MD. (2001). *Biochim. Biophys. Acta*, **1471,** M99–M108.

Powers CJ, McLeskey SW and Wellstein A. (2000). *Endocr. Relat. Cancer*, **7,** 165–197.

Rodriguez-Manzaneque JC, Lane TF, Ortega MA, Hynes RO, Lawler J and Iruela-Arispe ML. (2001). *Proc. Natl. Acad. Sci. USA*, **98,** 12485–12490.

Schlessinger J, Plotnikov AN, Ibrahimi OA, Eliseenkova AV, Yeh BK, Yayon A, Linhardt RJ and Mohammadi M. (2000). *Mol. Cell*, **6,** 743–750.

Soker S, Goldstaub D, Svahn CM, Vlodavsky I, Levi BZ and Neufeld G. (1994). *Biochem. Biophys. Res. Commun.*, **203,** 1339–1347.

Tang W, Nakamura Y, Tsujimoto M, Sato M, Wang X, Kurozumi K, Nakahara M, Nakao K, Nakamura M, Mori I and Kakudo K. (2002). *Mod. Pathol.*, **15,** 593–598.

Tumova S, Woods A and Couchman JR. (2000). *Int. J. Biochem. Cell Biol.*, **32,** 269–288.

Uno F, Fujiwara T, Takata Y, Ohtani S, Katsuda K, Takaoka M, Ohkawa T, Naomoto Y, Nakajima M and Tanaka N. (2001). *Cancer Res.*, **61,** 7855–7860.

Vlodavsky I, Bar-Shavit R, Ishai-Michaeli R, Bashkin P and Fuks Z. (1991). *Trends Biochem. Sci.*, **16,** 268–271.

Vlodavsky I, Friedmann Y, Elkin M, Aingorn H, Atzmon R, Ishai-Michaeli R, Bitan M, Pappo O, Peretz T, Michal I, Spector L and Pecker I. (1999). *Nat. Med.*, **5,** 793–802.

Vlodavsky I, Miao HQ, Medalion B, Danagher P and Ron D. (1996). *Cancer Metast. Rev.*, **15,** 177–186.

Yurchenco PD and Schittny JC. (1990). *FASEB J.*, **4,** 1577–1590.

Zcharia E, Metzger S, Chajek-Shaul T, Friedmann Y, Pappo O, Aviv A, Elkin M, Pecker I, Peretz T and Vlodavsky I. (2001). *J. Mammary Gland Biol. Neoplasia*, **6,** 311–322.

Zetser A, Bashenko Y, Miao HQ, Vlodavsky I and Ilan N. (2003). *Cancer Res.*, **63,** 7733–7741.